Fault direction identification utilizing new current-based index founded on rate of change of fault current

Electric Power Systems Research 201 (2021) 107511

Contents lists available at ScienceDirect

Electric Power Systems Research

journal homepage: www.elsevier.com/locate/epsr

Fault direction identification utilizing new current-based index founded on rate of change of fault current

Mohammad Sadegh Payam [a], Haidar Samet [a,b,*], Teymoor Ghanbari [c], Mohsen Tajdinian [a]

[a] School of Electrical and Computer Engineering, Shiraz University, Shiraz, Iran
[b] Department of Electrical Engineering, Eindhoven University of Technology, Eindhoven, The Netherlands
[c] School of Advanced Technologies, Shiraz University, Shiraz, Iran

ARTICLE INFO

Index terms:
Distributed generation
Distribution grid
Directional relay

ABSTRACT

The proliferation of Distributed Generations (DGs) in distribution networks has provided power system operation improvement while raising some protection challenges. Turning to bi-directional, the protection schemes of the deregulated distribution networks should be able to deal with an out-of-zone fault. More specifically, DGs impose bi-directional fault current and directional relay should be employed to identify correct fault direction so that the protective relays are prevented from mal-operation of out-of-zone fault. This paper introduces a current-based directional algorithm that utilizes a pre-fault current signal as the reference. This algorithm is designed based on the pre-fault current and rate of change of the fault current. As it can be inferred from the mathematical basis of the proposed method, it has low sensitivity to decaying DC and noise components. Also, the proposed index has a certain and straightforward range of variation between (-1, 1) for backward and forward fault direction, respectively. The performance of the proposed algorithm is evaluated for different scenarios such as variation of fault resistance, sampling frequency, and types of faults in three simulated systems and a laboratory test bench. The simulation and experimental evaluation results show the accuracy and speed of the proposed algorithm in comparison with similar algorithms.

List of symbols

i_{pf}	Pre-fault current
k	Sample number
i	Current signal
$I_{max,pf}$	Peak of pre-fault current
$i_{pf.n}$	Normalized pre-fault current
β_{pf}	Phase of pre-fault current
i_{df}	Fault current
β_{df}	Phase of during-fault current
$I_{max,df}$	Peak of fault current
$i_{df.n}$	Normalized during-fault current
i_{df}^{prime}	Derivative of during-fault current
$i_{df.n}^{prime}$	Normalized derivative of during-fault current
τ	Time constant of short circuit
ACI	Interim Variable
$MACI$	Proposed directional Index
ω	Angular frequency
$\varnothing$	Difference between the phases of during and pre-fault currents
I_n	Rated pre-fault current
v	Pre-fault voltage signal
γ	Source voltage angle
θ	Impedance angle
T	One cycle time
k	Sample No.
N	Number of one cycle samples
s	DFIG slip
V_R	Pre-fault voltage of a DFIG
R	Transient resistance of DFIG
X_{df}^{prime}	Transient reactance of DFIG
R_{cb}	Crowbar resistance of DFIG
T_{cb}	Transient time constant of DFIG
Ta	Stator time constant of DFIG
$f_{S.F}$	Fundamental frequency of stator fault

* Corresponding author.
E-mail addresses: samet@shirazu.ac.ir, h.samet@tue.nl (H. Samet).

https://doi.org/10.1016/j.epsr.2021.107511
Received 31 March 2021; Received in revised form 22 July 2021; Accepted 7 August 2021
Available online 17 August 2021

1. Introduction

Expansion of the utilization of Distributed Generations (DGs) in distribution networks has led to its many benefits including loss reduction, improvement of voltage profile, increase in reliability, and reduction of environmental pollutants [1, 2]. Despite these advantages, DGs have imposed some protection challenges in distribution networks. Increasing the short-circuit level and changing the arrangement of distribution networks from unidirectional to bi-directional are known as the most influential challenges [3, 4]. Some protection strategies have been introduced to deal with enhanced short circuit levels [5, 6]. However, turning to bi-directional networks, maloperation of the protection schemes in such networks should be prevented in faults outside the protection zone. It means the protection schemes require directional relays to detect the fault direction in presence of DGs [7].

Surveying the previous publications in the directional protection algorithms, the algorithms can be divided into four groups from the analysis domain including (A) time-domain analysis, (B) frequency-domain analysis, (C) time-frequency analysis, and (D) machine learning technique [8].

Regardless of the domain analysis types, surveying the literature reveals that the directional protection algorithms should be able to deal with challenges including requirement window of data (e.g. sub-cycle or full-cycle window of data), dependency on the input signal (e.g. voltage, current, or both of them), noise sensitivity, sensitivity to the decaying DC component in the current signal.

According to the above-mentioned categorizations:

- The algorithms based on the correlation function [9, 10], and the algorithm based on superimposed components [11, 12] are some of the examples of the time-domain analysis. While time-domain analysis has a high-speed response, these algorithms suffer from low accuracy, sensitivity to noise, and the decaying DC component. Note that these algorithms can be implemented with a relatively low sampling rate.
- Frequency-domain analysis including positive sequence impedance [13] and the phase difference [14] algorithms, employs the fundamental phasor components of voltage and current to determine fault direction. Owing to employing the fundamental phasor component, these algorithms are generally reliable against noise, and decaying DC component of fault current comparing with time-domain algorithms. In these algorithms, the fundamental phasor components are generally estimated by some frequency analysis tools like Fourier Transform (FT) or Fast Fourier Transform (FFT), which induce a full-cycle delay in the detection process. As a result, the fault direction detection speed of these algorithms is rather low. Note that these algorithms are more accurate than time-domain algorithms.
- Combined time-frequency analysis tools such as wavelet transform [15, 16], provide higher speed in comparison with the other categories. Unfortunately, these algorithms suffer from high sampling frequency, high sensitivity to noise, and the decaying DC component.
- The fourth group includes machine learning techniques which are based on Neural Networks (NN) [17], Modular NN [18], Elman NN [19], and multilayer feed-forward NN [20]. These algorithms have acceptable speed and accuracy but they are complex and uninterpretable. Moreover, considerable training data are required to be trained. Furthermore, with a change in power system parameters, the training procedure should be repeated.

In general, most of the above-mentioned algorithms use voltage and current signals as input. The use of voltage signals in algorithms, in addition to increasing the cost, leads to problems in detecting the direction in the event of a fault near the relay. In other words, at fault close to the relay, the voltage signal drops significantly, which can lead to incorrect operation of directional algorithms. As a result, it can be concluded that employing the current-based algorithms can prevent the difficulties of the voltage-drop issues in the case of the fault near the directional relays. However, it should be noted that the current-only-based algorithms should be designed to have no sensitivity to the decaying DC component.

The latter-discussed issues in the previously published algorithms, this paper puts forward an efficient current-based directional algorithm.

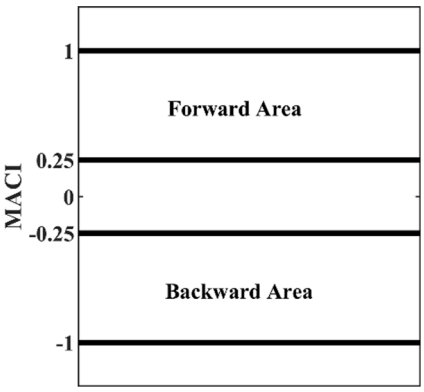

Fig. 1. Forward and backward detection area.

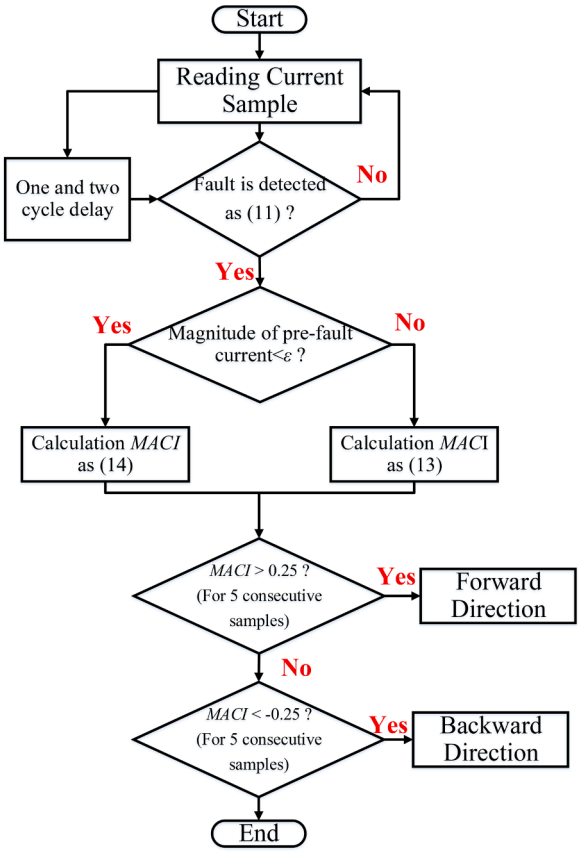

Fig. 2. The flowchart of the proposed algorithm.

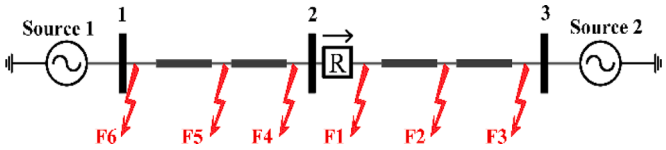

Fig. 3. The test system with two sources.

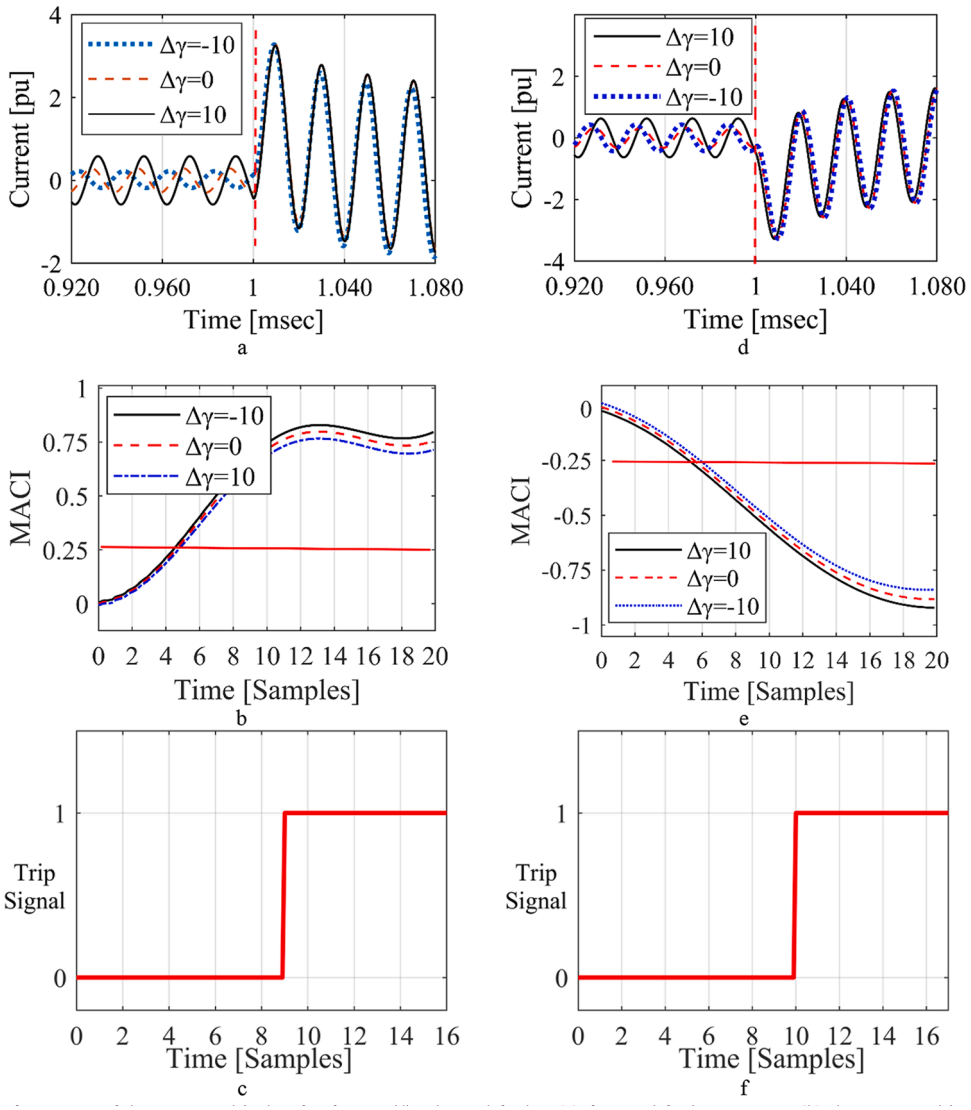

Fig. 4. Performance of the proposed index for forward/backward faults, (a) forward faults currents, (b) the proposed index for the forward fault currents, (c) detection signal, (d) the backward fault currents, (e) the proposed index for the backward fault currents, (f) detection signal.

Table 1
Accuracy of the algorithms for different sampling frequency

Sampling Frequency kHz)	Required Time (ms)		Error (%)
	Max	Average	
1	11	9.5	2.1
2	5.6	4.9	1.15
5	2.3	1.9	0.98
10	1.09	0.94	0.75

The proposed directional index is designed based on the pre-fault current and rate of change of fault current and this algorithm belongs to the time-domain analysis group. The summary of the contributions of the paper are as follows:

- As discussed, the time-domain type of the direction fault detection algorithms suffers from signal transients, especially decaying DC components in the current-based algorithms. It has been Mathematically proven that, due to the use of the rate of change of fault current signal, the proposed index has very little sensitivity to the decaying DC component. As a result, unlike [21], it has immunity against the decaying DC component in the fault current signal.
- Unlike [22-24], the proposed index does not suffer from voltage-drop issues for fault near the directional algorithm.
- In the proposed index, a half-cycle moving average indicator is employed and as a result, the presence of the proposed index reduces the sensitivity of the algorithm to noise.
- Comparing to the state-of-the-art algorithms, the proposed method requires a low sampling rate. Also, low-complexity formulations indicate that the proposed index has a low computational burden compared with the state-of-the-art algorithms.

The rest of the paper is organized as follows: the proposed algorithm basis and formulations are provided in section 2. Section 3 discusses the proposed algorithm implementation and requirements. Simulation and experimental results and discussions are provided in Sections 4 and 5. Finally, Section 6 provides conclusions.

2. Proposed algorithm basis and formulations

This paper tries to provide a directional index that is designed based on the pre-fault current and rate of change of fault current. This section is dedicated to the mathematical basis of the derived proposed index and the operational region for fault direction detection.

Table 2
The results of the proposed algorithm for different fault resistances

Fault Type	$\Delta\delta$	Fault Location	R_F (Ω)	Average Required Time (samples)	Detected Direction
Ag	10	F1-F3	0	4.95	Forward
			2.5	5.02	
			5	5.12	
			15	5.14	
			20	5.22	
			50	5.31	
			100	5.36	
		F4-F6	0	4.93	Backward
			2.5	4.99	
			5	5.06	
			15	5.15	
			20	5.17	
			50	5.21	
			100	5.30	
ABg	10	F1-F3	0	4.96	Forward
			2.5	4.98	
			5	5.12	
			15	5.14	
			20	5.22	
			50	5.27	
			100	5.34	
		F4-F6	0	5.01	Backward
			2.5	5.12	
			5	5.13	
			15	5.19	
			20	5.23	
			50	5.31	
			100	5.36	
ABCg	10	F1-F3	0	4.91	Forward
			2.5	4.98	
			5	5.03	
			15	5.12	
			20	5.16	
			50	5.22	
			100	5.29	
		F4-F6	0	4.97	Backward
			2.5	5.02	
			5	5.11	
			15	5.13	
			20	5.15	
			50	5.27	
			100	5.29	

Table 3
The results of the proposed algorithm for zero pre-fault current situations

NO.	Fault Type	Fault Location	R_F (Ω)	Average Required Time (samples)	Detected Direction
1	Ag	F2	0	4.65	Forward
2			50	5.13	
3		F5	0	4.72	Backward
4			50	4.93	
5	ABg	F2	0	4.70	Forward
6			50	4.92	
7		F5	0	5.08	Backward
8			50	5.12	
9	ABCg	F2	0	4.23	Forward
10			50	5.08	
11		F5	0	4.41	Backward
12			50	5.42	

2.1. Fault current normalization

It is assumed that before fault occurrence, the current signal is expressed as follows:

$$i_{pf} = I_{max,\ pf} cos(\omega t - \beta_{pf}) \tag{1}$$

where *pf* stands for the pre-fault interval. In (1), $I_{max,pf}$ and β_{pf} are the peak and the phase of pre-fault current, respectively. Normalizing i_{pf}, the following expression is concluded:

$$i_{pf,n} = \frac{i_{pf}}{I_{max,\ pf}} = cos(\omega t - \beta_{pf}) \tag{2}$$

During a fault, the short circuit current signal includes a decaying DC component [25]. The fault current signal is mathematically expressed as follows:

$$i_{df} = I_{max,df}\cos(\omega t - \beta_{df}) - I_{max,df} cos(\beta_{df}) e^{-t/\tau} \tag{3}$$

where subscript *df* stands for the during-fault interval. In (3), $I_{max,df}$ and β_{df} are the peak and the phase of short circuit current, respectively. Also, τ is the time constant of the short-circuit current. Applying derivation on (3), it can be concluded:

$$\frac{di_{df}}{dt} = i'_{df} = -I_{max,df}\omega\sin(\omega t - \beta_{df}) + \frac{I_{max,df}}{\tau} cos(\beta_{df}) e^{-t/\tau} \tag{4}$$

Normalizing i_{df}^{prime}, the following can be concluded:

$$i'_{df,n} = \frac{i'_{df}}{-I_{max,df}\omega} = \sin(\omega t - \beta_{df}) - \frac{1}{\tau\omega} cos(\beta_{df}) e^{-t/\tau} \tag{5}$$

2.2. The proposed index for fault direction identification

To obtain the proposed index for the fault direction identification, by multiplying $i_{pf,n}$ and $i_{df,n}^{prime}$, it can be concluded:

$$\begin{aligned} CI &= i_{pf,n} i'_{df,n} \\ &= \cos(\omega t - \beta_{pf}) \left[\sin(\omega t - \beta_{df}) - \frac{1}{\tau\omega} cos(\beta_{df}) e^{-t/\tau}\right] \\ &= \cos(\omega t - \beta_{df})\sin(\omega t - \beta_{df}) - \frac{1}{\tau\omega}\cos(\beta_{df}) cos(\omega t - \beta_{pf}) e^{-t/\tau} \end{aligned} \tag{6}$$

Applying integration over half-cycle of the period in (6), the following is concluded:

$$\begin{aligned} ACI &= \int_0^{\frac{T}{2}} i_{pf,n} i'\, df, ndt \\ &= \int_0^{\frac{T}{2}} \frac{1}{2}\left[\sin(2\omega t - \beta_{pf} - \beta_{df}) - sin(\beta_{df} - \beta_{pf})\right] dt \\ &- \int_0^{\frac{T}{2}} \frac{1}{\tau\omega} cos(\beta_{df}) cos(\omega t - \beta_{pf}) e^{-t/\tau} dt \end{aligned} \tag{7}$$

where *ACI* is the average of *CI* over half-cycle of the fundamental period. Simplifying (7), the following is concluded:

$$\begin{aligned} ACI = &-\frac{T}{2}\sin(\beta_{df} - \beta_{pf}) \\ &-\frac{\frac{cos(\beta_{df})cos(\beta_{pf})}{\tau^2\omega}\left(1 + e^{-T/2\tau}\right) + \frac{cos(\beta_{df})sin(\beta_{pf})}{\tau}\left(1 + e^{-T/2\tau}\right)}{\omega^2 + \left(\frac{1}{\tau}\right)^2} \end{aligned} \tag{8}$$

In (8), the presence of $\omega^2 + \left(\frac{1}{\tau}\right)^2$ in the denominator leads to the reduction of the second part, so this term can be removed and the following can be concluded:

$$ACI \cong -\frac{T}{2} sin(\beta_{df} - \beta_{pf}) = -\frac{T}{2} sin(\varnothing) \tag{9}$$

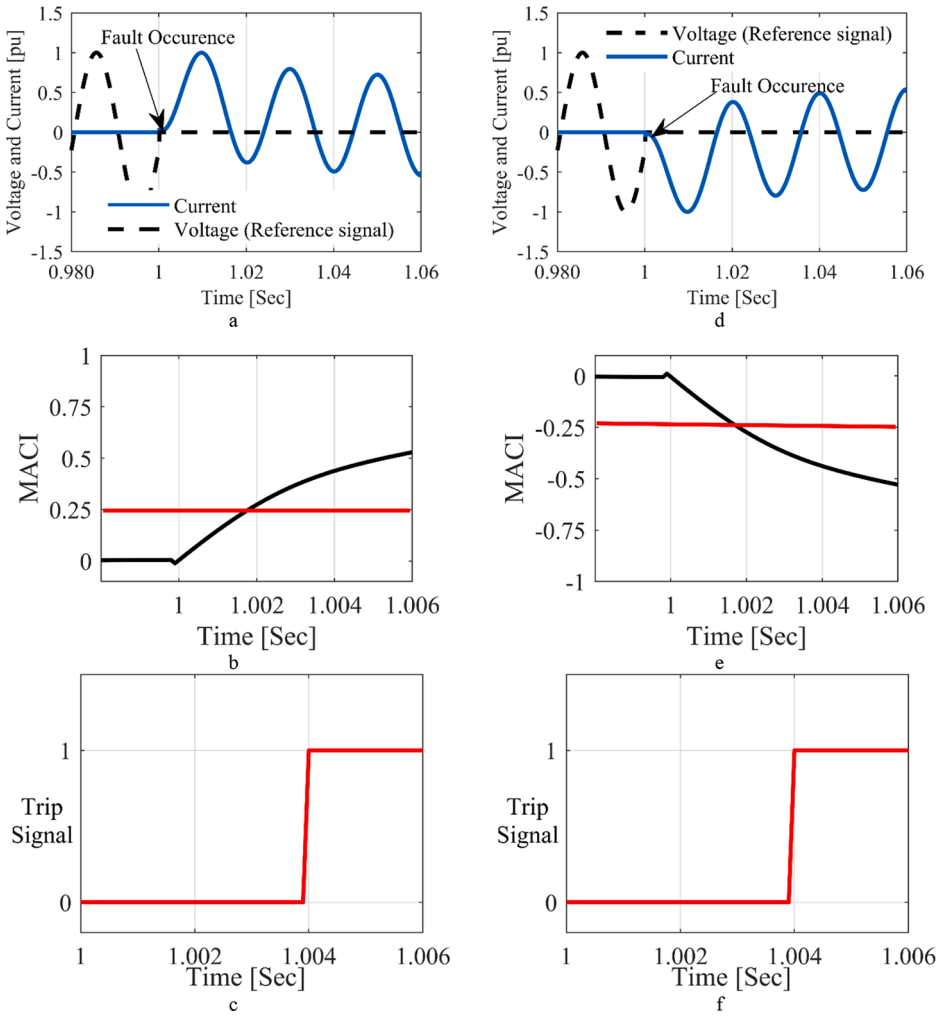

Fig. 5. Performance of the proposed index for zero pre-fault current, (a) forward fault current, (b) the proposed index for the forward fault current, (c) detection signal, (d) the backward fault current, (e) the proposed index for the backward fault current, (f) detection signal

Table 4
Reference parameters of the DIST-C HIAF MODEL [28]

Case NO.	Fault location	Material and humidity of the ground surface or object	Parameters of DIST-C model OFS (kV)	EXT (kΩ)	DUR (ms)	RT (kΩ)
1	F2	wet reinforced concrete	-1.461	0.1578	7.402	100
2	F5	wet reinforced concrete	-1.461	0.1578	7.402	100

Multiplying *ACI* by $2/T$, Modified *ACI* is concluded as follows:

$$MACI = \frac{2}{T}ACI = -sin(\varnothing) \tag{10}$$

Three possible regions including the normal operation of the power system condition, fault in the forward direction, and fault in the backward direction are considered. In normal conditions, the power factor of typical loads in distribution networks is in the range of 0.8 lag to 1. As a result, β_{pf}, the phase of pre-fault current, is approximately between -36° and 0°.

According to [25], the permissible range of $\varnothing = \beta_{df} - \beta_{pf}$ for the forward faults is considered between –120° and –15°. The afore-mentioned range is obtained considering impedance angle (θ) range between 45° and 90°, and source voltage angle (γ) range between 0° and 30° for positive and negative power flow states, respectively, and the pre-fault current (β_{pf}) is in the range of -36° and 0°. As a result, the range of *MACI* changes for the forward faults between 0.25 and 1. Similarly, the range of *MACI* changes for backward faults between -0.25 and -1. The range of *MACI* is shown in Fig. 1.

2.3. Zero pre-fault current situations

The zero pre-fault current situations such as switch onto fault is a challenge in the current-based methods. To deal with zero pre-fault current situations, the proposed method employs an auxiliary criterion to improve the performance of the proposed method in zero pre-fault current situations. In order to discriminate the zero pre-fault current situations and utilize the auxiliary criterion, after the fault detection, the magnitude of the pre-fault current is compared with a small value like ε (ε is set in $0.001In$). For the pre-fault current less than ε, the pre-fault voltage waveform is considered as the reference signal and the same procedure for *MACI* index used to determine fault direction.

3. Proposed algorithm implementation and requirements

3.1. Detection of fault occurrence

At the first step, it is needed to detect fault occurrence. In this paper, a common and simple fault detection approach is used [26]. In this approach, fault occurrence is detected when the following condition is

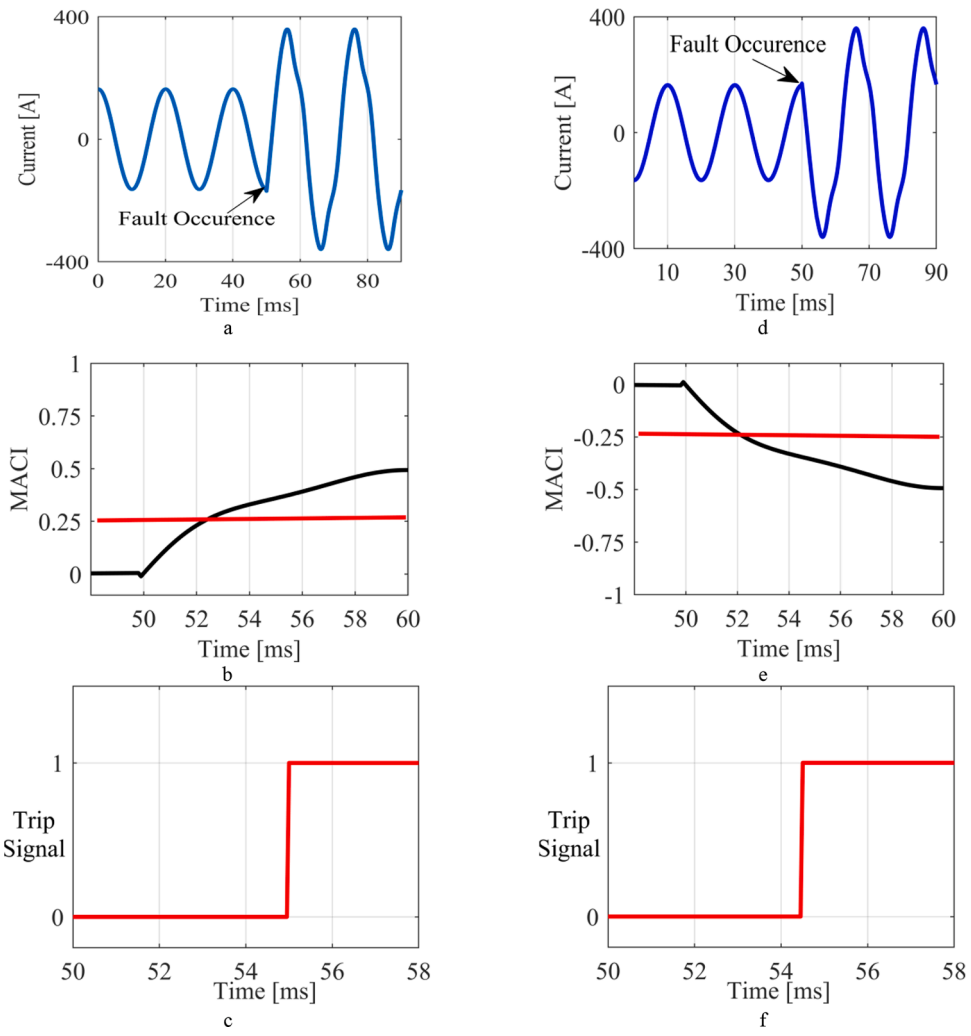

Fig. 6. Performance of the proposed index for high impedance arcing faults, (a) forward fault current, (b) the proposed index for the forward fault current, (c) detection signal, (d) the backward fault current, (e) the proposed index for the backward fault current, (f) detection signal

Table 5
Effect of system frequency variation on the performance of the proposed algorithm

Slip	Case Studies	Fault Location	Fault Resistance (Ω)	Average Required Time (ms)	Accuracy (%)
-0.2	30	F1- F6	0-100	5.44	98.67
-0.1	30	F1- F6	0-100	5.39	99.05
0	30	F1- F6	0-100	5.12	99.12
0.1	30	F1- F6	0-100	5.23	98.99
0.2	30	F1- F6	0-100	5.27	98.84
0.3	30	F1- F6	0-100	5.40	98.57

satisfied:

$$||i[k]-i[k-N]|-|i[k-N]-i[k-2N]|| \geq 0.2I_n \quad (11)$$

where k is the sample number, N is the number of samples in one cycle, and I_n is the rated current. Also, $i[k]$ is the current sample, $i[k-N]$ is its corresponding sample in one previous cycle, and $i[k-2N]$ is the corresponding sample in two previous cycles. In this approach, by subtracting the values of these samples and comparing the result with $0.2I_n$, fault is detected.

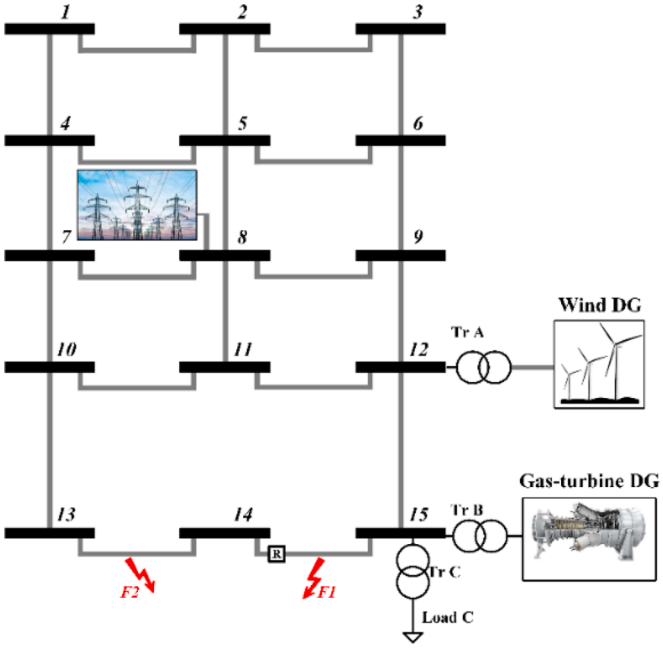

Fig. 7. Single line diagram of a 15-bus system

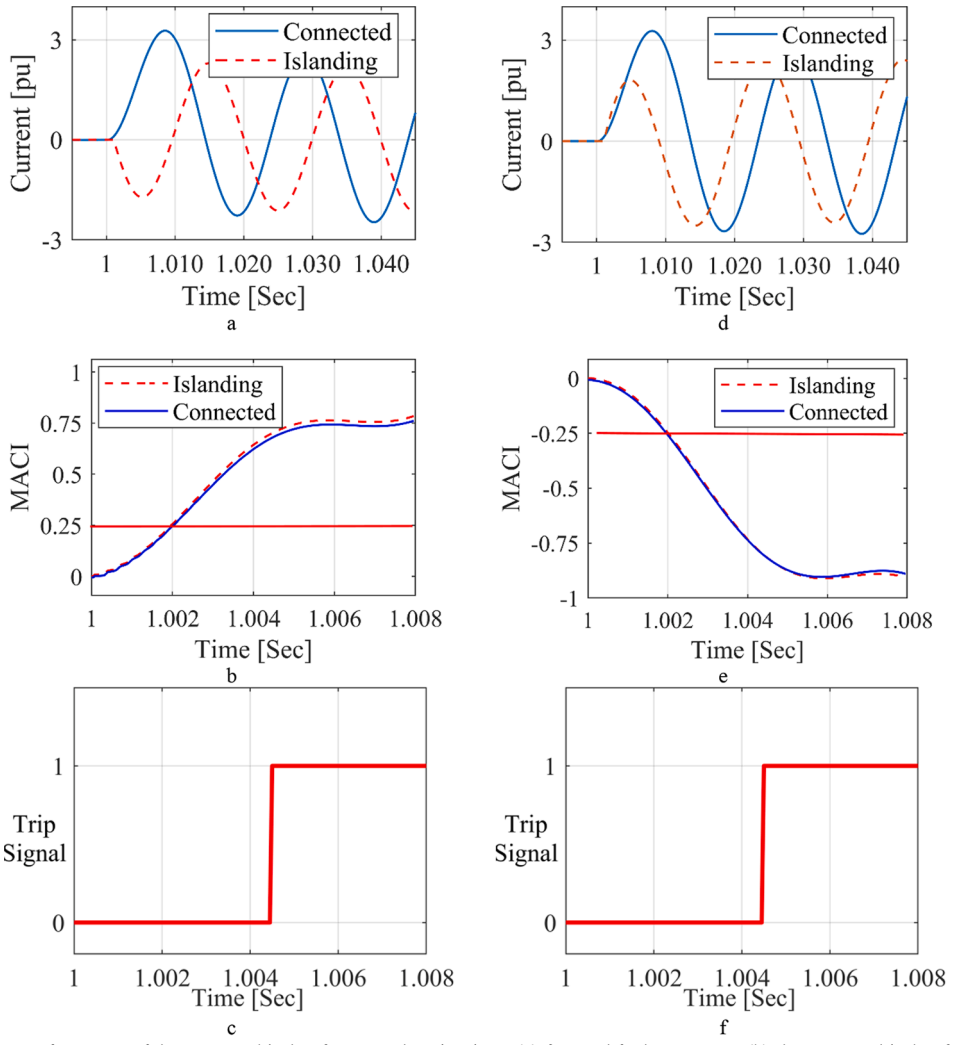

Fig. 8. Performance of the proposed index for F1 and F2 in Fig.7, (a) forward faults currents, (b) the proposed index for the forward fault currents, (c) detection signal, (d) the backward fault currents, (e) the proposed index for the backward fault currents, (f) detection signal

Table 6
Evaluation results of the proposed algorithm in Fig.7

Fault Type	Fault Location	Slip	Grid-Connected Mode Average Time (ms)	Grid-Connected Mode Accuracy (%)	Islanded Mode Average Time (ms)	Islanded Mode Accuracy (%)
Ag	F1	-0.2	5.28	98.61	5.57	98.24
		0	5.12	99.12	5.42	99.05
		0.2	5.34	98.71	5.67	98.54
	F2	-0.2	5.31	98.65	5.49	98.12
		0	5.09	99.09	5.33	98.95
		0.2	5.39	98.68	5.70	98.29
ABg	F1	-0.2	5.35	98.56	5.61	98.19
		0	5.11	99.25	5.23	99.16
		0.2	5.41	98.78	5.66	98.64
	F2	-0.2	5.34	98.52	5.72	98.42
		0	5.12	99.17	5.35	98.98
		0.2	5.38	98.74	5.47	98.57
ABCg	F1	-0.2	5.21	98.69	5.39	98.64
		0	4.98	99.38	5.20	99.11
		0.2	5.18	98.79	5.58	98.62
	F2	-0.2	5.26	98.54	5.56	98.43
		0	5.02	99.45	5.21	99.21
		0.2	5.17	99.02	5.49	98.89

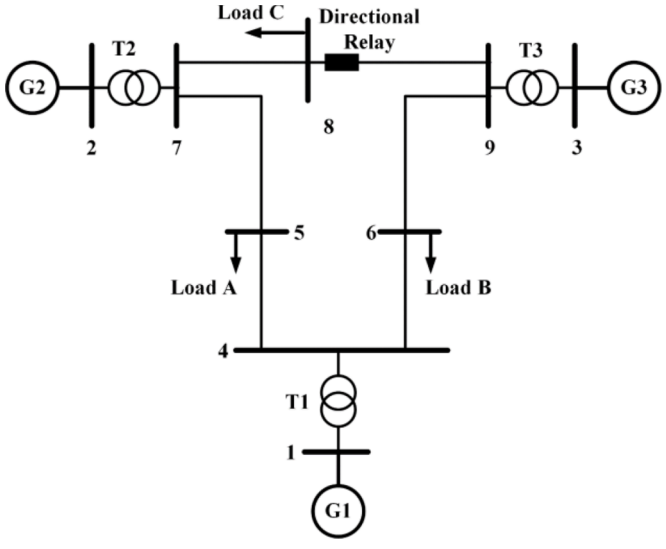

Fig. 9. The single line diagram of 9 bus IEEE test system

Table 7
Fault scenarios data

Case NO.	Fault resistance (ohm)	Fault Location
1	0	front
2	0	behind
3	5	front
4	5	behind
5	50	front
6	50	behind

3.2. Detection of fault direction

To implement the proposed index, two data moving windows including memory and analysis windows are considered during the implementation. The current samples in the memory window are considered as the reference signal. It is considered that the two windows length is N samples and the memory window is delayed N samples relevant to the analysis window. In this method, the data of the analysis window is applied to the derivative block. Then, the output of the derivative block and the reference signal are multiplied and the summation of the results is considered as ACI index. Now, the calculated *ACI* index is multiplied by 2 and the *MACI* index is calculated.

The analysis window is moved sample by sample and the signal of *MACI* is continuously calculated. This signal changes between (-0.25, 0.25) for normal conditions. If it moves to the range of (0.25, 1) and at least 5 samples remain in this range, the algorithm detects a forward fault. If the proposed signal moves to the range of (-0.25, -1) and at least 5 samples remain in this range, the algorithm detects a backward fault.

Here, the implementation of the proposed algorithm for fault direction identification is shown in Fig. 2. In summary, the following steps are followed up to determine the fault direction in this method:

Step 1: Fault detection

Step 2: Comparing the pre-fault current with ε

If the pre-fault current is greater than ε, go to step3 otherwise go to step 4.

Step 3: *MACI* calculation based on pre-fault current

The *ACI* is calculated once each current sample is updated. The *ACI* is calculated as follows:

$$ACI[k] = \sum_{k=1}^{N} i'[k]i[k-N] \tag{12}$$

Moreover, the *MACI* is calculated for each sample of the fault current signal as follows:

$$MACI[k] = \left(\frac{2}{T}\right)ACI[k] \tag{13}$$

Step 4: *MACI* calculation based on pre-fault voltage

The *MACI* is calculated as follows:

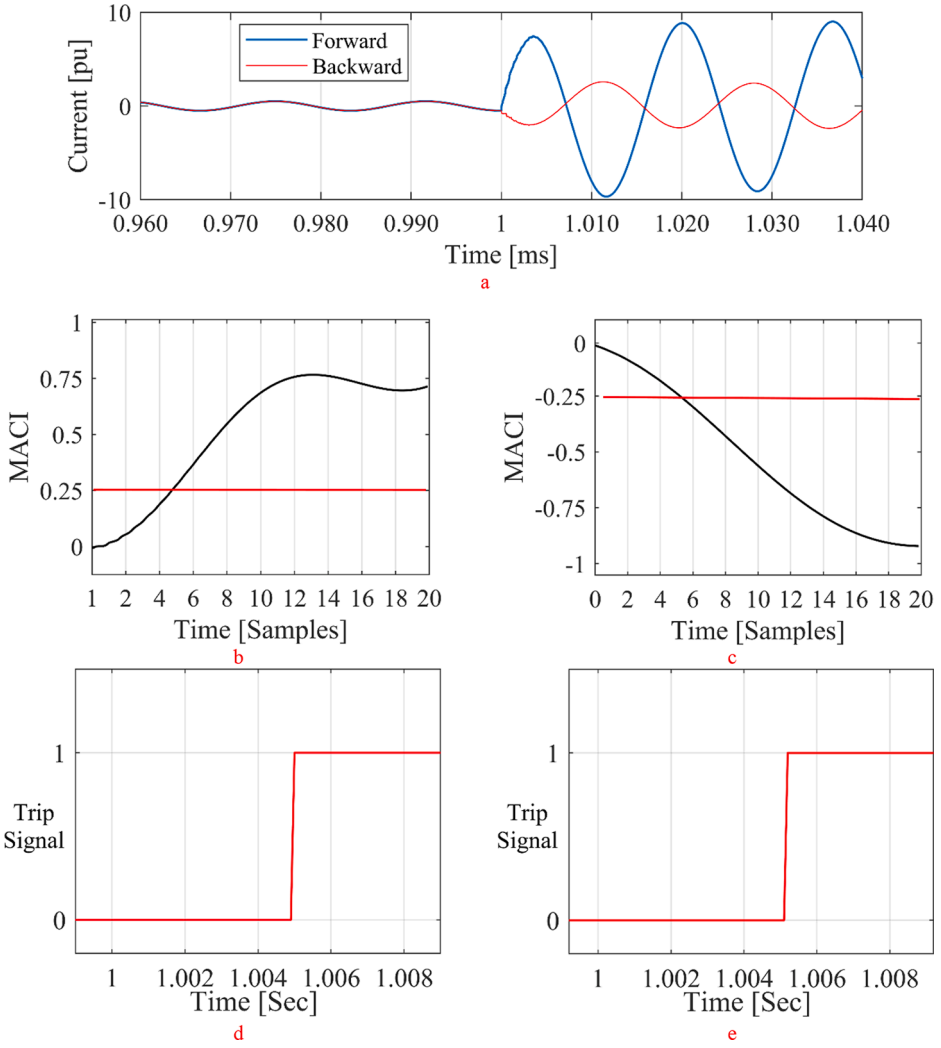

Fig. 10. The performance of the proposed index for case 1&2, (a) forward and backward fault current, (b) the proposed index for the forward fault, (c) the proposed index for the backward fault, (d) detection signal for the forward fault, (e) detection signal for the backward fault

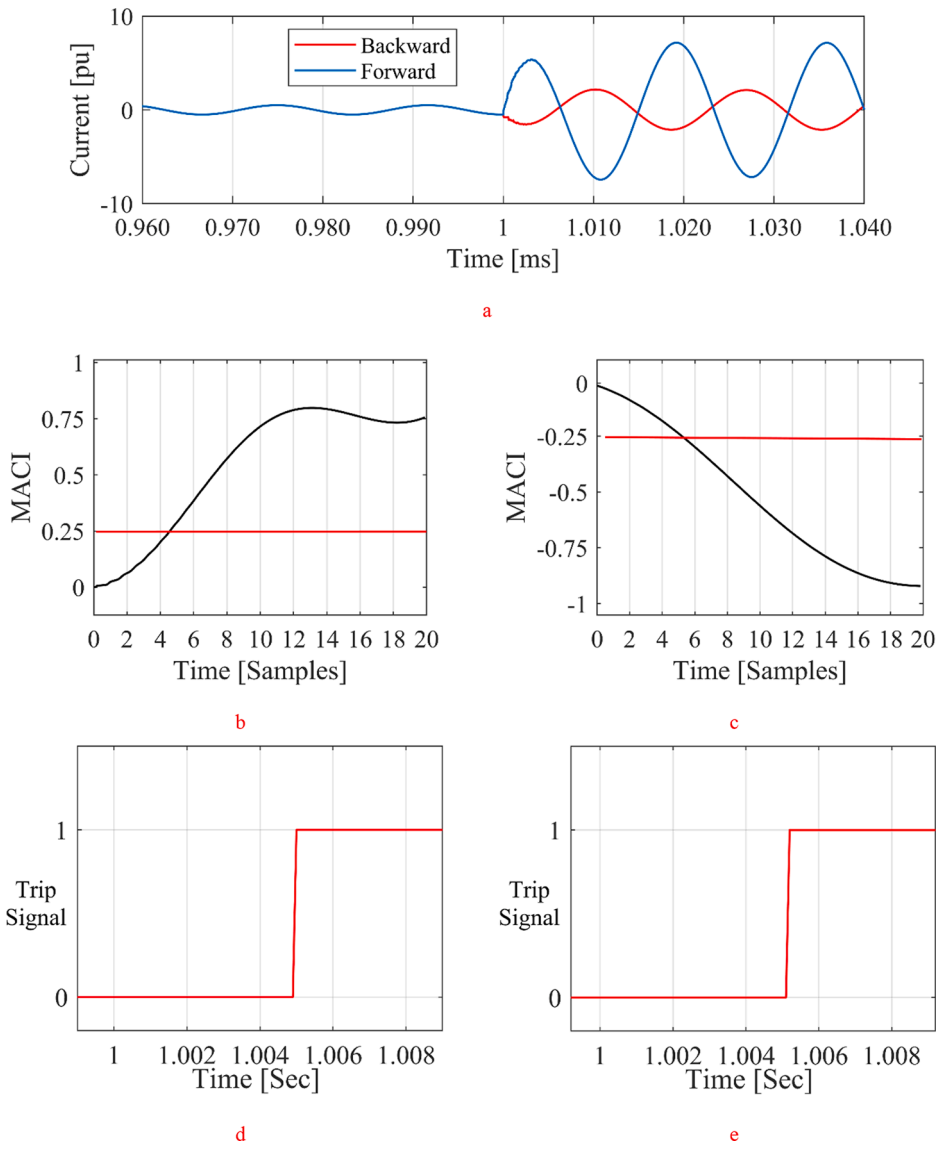

Fig. 11. The performance of the proposed index for case 3&4, (a) forward and backward fault current, (b) the proposed index for the forward fault, (c) the proposed index for the backward fault, (d) detection signal for the forward fault, (e) detection signal for the backward fault

$$MACI[k] = \left(\frac{2}{T}\right)\sum_{k=1}^{N} i'[k]v[k-N] \tag{14}$$

Step 5: Comparing the calculated index with the detection regions

If the forward region remains (0.25, 1) for five consecutive samples, the algorithm identifies the forward fault direction. Also, if *MACI* falls in the backward region (-0.25, -1) for five consecutive samples, the algorithm identifies the backward fault direction.

4. Performance evaluation

Here, the performance of the proposed fault direction identification index is evaluated. The performance evaluation is performed using three simulated test systems in PSCAD. Also, employing a programmable processor, the proposed algorithm is implemented to evaluate the computational efficiency of the proposed algorithm. Eventually, the performance evaluation under experimentally recorded fault currents is provided.

4.1. Simulation results for two sources test system

Fig. 3 provides a simple two-bus test system operating at 20 kV. The system has two sources, one is considered as an upstream network, and the other as a DG source. In this study, two types of DG are simulated, a synchronous generator, and a Doubly Fed Induction Generator (DFIG). The performance of the proposed algorithm is evaluated in the presence of these two sources. In sections 1 to 3, the DG type is the synchronous generator and in section 4, the DG type is the DFIG.

4.1.1. Performance assessment for negative and positive normal power flow

To assess the performance of the proposed index for negative and positive normal power flow states, 1 MW synchronous generator is considered in Fig.3. The details of this DG are presented in [27]. The type and resistance of all faults were assumed to be three phases and zero, respectively, and the fault inception instants were considered, randomly. In all simulations, DG is modeled as a series voltage source with a reactance (transient reactance). If $\Delta\gamma$ is defined as the difference between the upstream and DG source voltage angles, positive and negative $\Delta\gamma$ mean positive and negative normal power flow states, respectively.

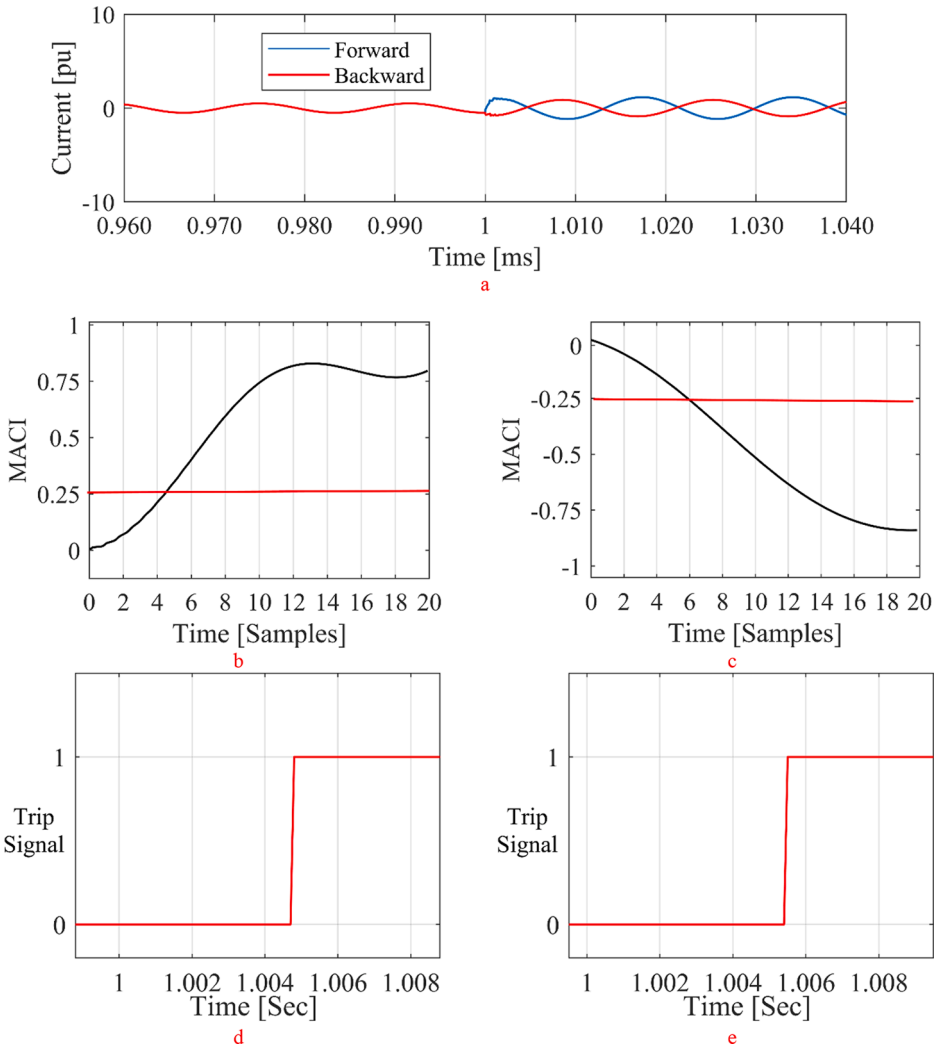

Fig. 12. The performance of the proposed index for case 5&6, (a) forward and backward fault current, (b) the proposed index for the forward fault, (c) the proposed index for the backward fault, (d) detection signal for the forward fault, (e) detection signal for the backward fault

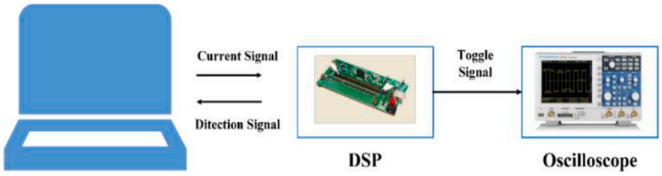

Fig. 13. The schematic of the employed test bench

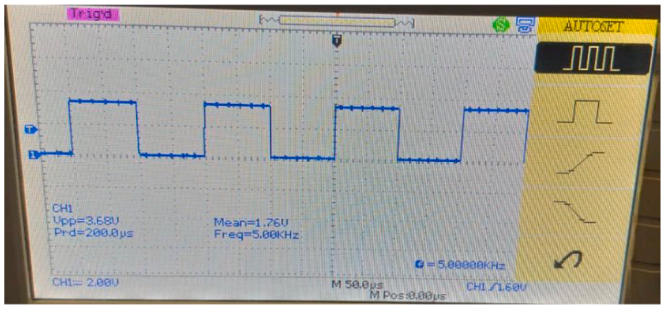

Fig. 14. Toggle signal of the proposed method

Figs. 4.a and d illustrate different forward and backward fault current signals considering positive and negative normal power flow states, respectively. As can be seen in Figs. 4.c and f, the *MACI* identified the fault direction in fewer than 10 samples. Note that the sampling frequency is selected as 2 kHz, and as a result, the average required time to detect the direction will be 5 ms.

4.1.2. *Performance assessment for different sampling frequencies*

This section is dedicated to evaluating the performance of a protection algorithm under different sampling frequencies. Here, the sampling frequency is changed in the range of 1 to 10 kHz as Table 1. In order to evaluate the performance of the algorithm at each sampling frequency, 100 different scenarios have been simulated including different fault resistances, normal power flows, fault locations, and fault types. The results of this section are presented in Table 1. To evaluate the accuracy of the methods, a percentage error index is defined as follows:

$$\%Error = \frac{Number\ of\ false\ discrimination}{total\ number\ of\ faults} \times 100 \tag{15}$$

The results show that the algorithm has an accuracy of about 98% for 1 kHz sampling frequency, which is acceptable but at this frequency, the speed of the algorithm is relatively low. By increasing the sampling frequency to 2 kHz, the average required time is about 5 ms and the accuracy is about 99%, which are acceptable. It is noteworthy that

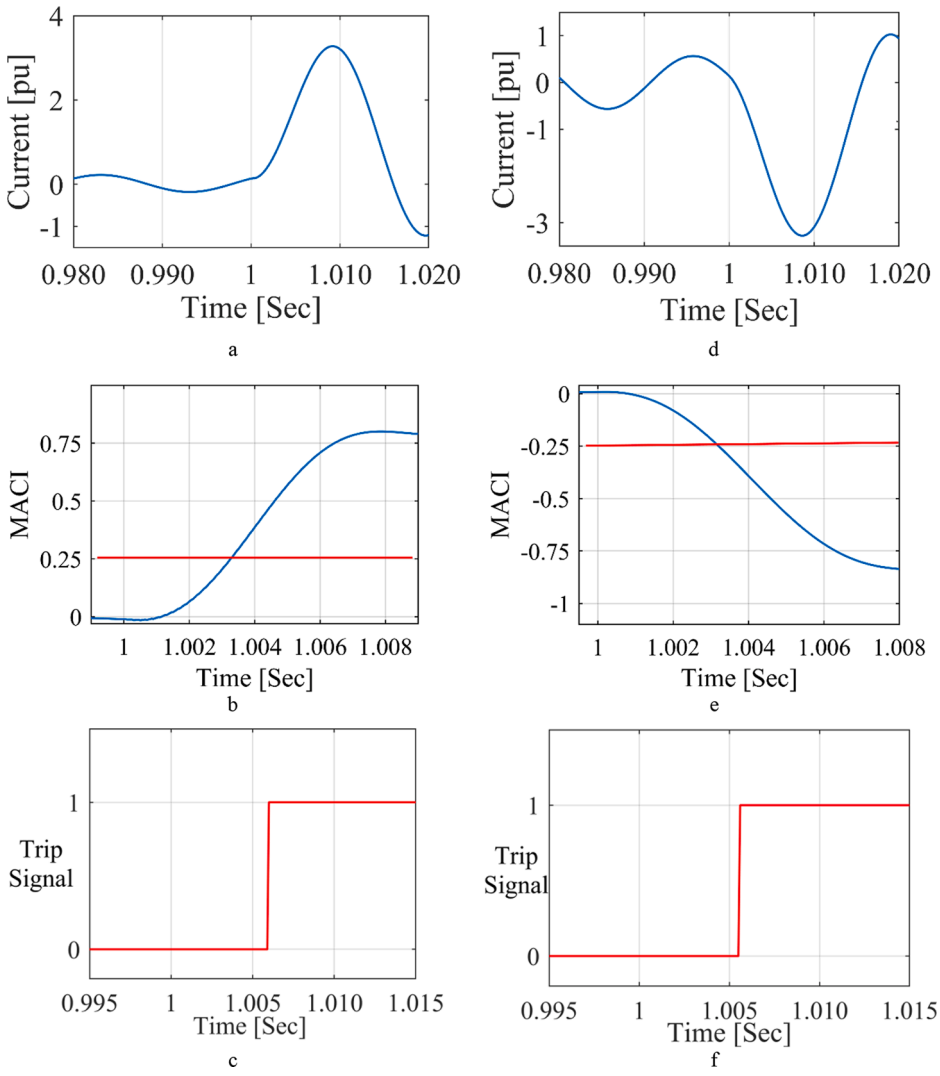

Fig. 15. Results of DSP implementation of the proposed index, a) forward current signal, b) proposed index, c) detection signal, d) backward current signal, e) proposed index, f) detection signal

although the accuracy of sampling has increased with increasing frequency, this leads to a higher computational burden. As a result, the sampling frequency is selected 2 kHz.

4.1.3. Performance assessment for different fault types, locations, and resistances

This section provides the assessment of the proposed index for different fault types, locations, and resistances. Multiple fault scenarios are simulated considering the fault resistance variations between 0 and 100 ohms. The locations of F1, F2, and F3 are considered for the forward faults, and the locations of F4, F5, and F6 are considered for backward faults, as shown in Fig. 3. Also, different fault types are considered including single-phase, two-phase and three-phase faults. The results of this section are presented in Table 2. From this table, it is concluded that the proposed algorithm has acceptable accuracy and speed in detecting fault direction in different scenarios.

The average detection time in the worst case is 5 ms and the lowest operating accuracy is 97.6% that are acceptable. The results show that although the speed of the algorithm decreased with increasing fault resistance, in all cases the detection time was less than 5.5 ms (about a quarter of a cycle at a nominal frequency of 50 Hz).

4.1.4. Effect of zero pre-fault current

In order to simulate zero pre-fault current situation, sources 1 and 2 are disconnected in cases of forward and backward faults, respectively. Therefore, the current magnitude is near to zero before the fault occurrence. Upon fault occurrence, the current magnitude increases, and the fault detection unit can detect it. In this situation, *MACI* index is calculated as (14). Table 3 shows some of the results for zero pre-fault current situations in which some conditions are changed to evaluate all of the possible fault situations. The results confirm that the proposed method can preserve its performance in case of zero pre-fault current situations, as well.

Figs. 5.a and d illustrate forward and backward fault current signals considering cases 2 and 4 of Table 3, respectively. As observed in Figs. 5. c and f, the *MACI* identified the fault direction in fewer than 5 ms.

4.1.5. Performance assessment of the proposed algorithm for high impedance arcing fault

To assess the performance of the proposed method for high impedance faults (HIFs), some scenarios are provided in the following. For this purpose, an accurate model of arc so-called distortion-controllable (DIST-C) HIF model is selected for the simulation of HIF that accurately reflects the variations of nonlinear distortions under different fault conditions [28]. In this model, there are three arc parameters of *DUR*, *OFS*, and *EXT*, which are meant to control the duration, offset, and extent of the distortions, respectively. During HIFs, the fault voltages usually experience little changes and remain sinusoidal due to the high

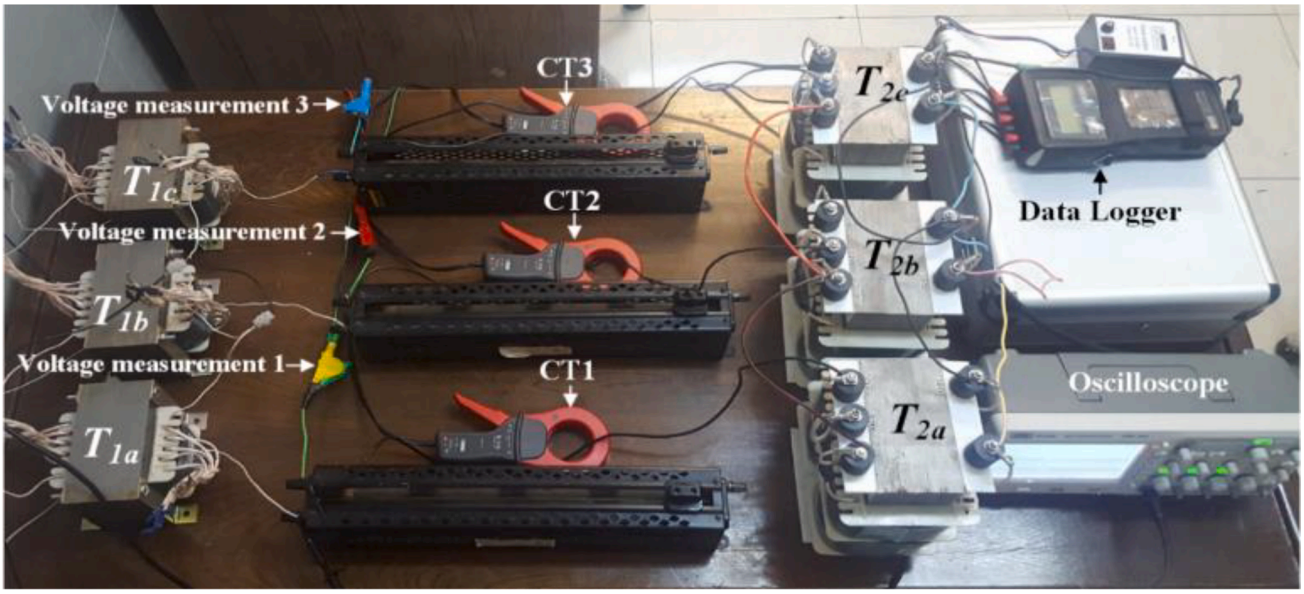

a

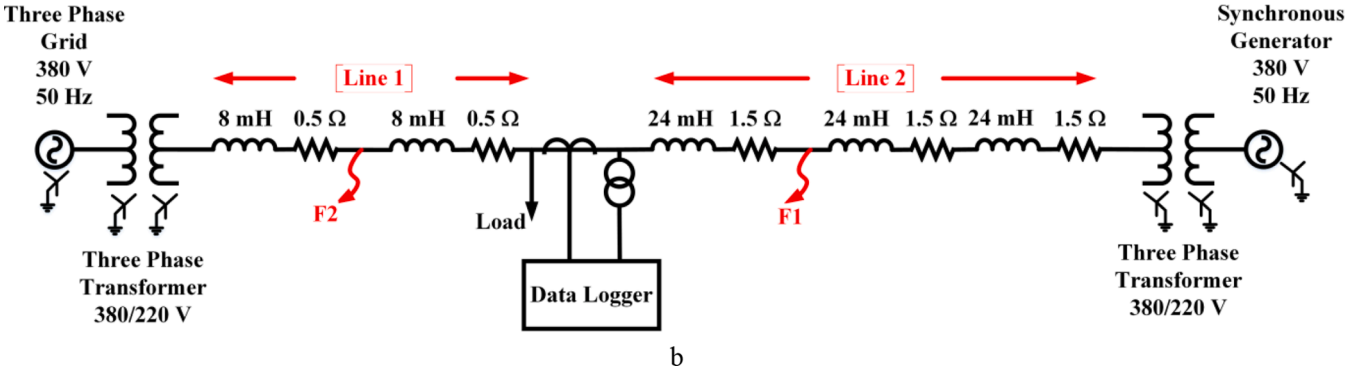

b

Fig. 16. a) Laboratory test bench, b) Single-line diagram of laboratory test bench

grounding resistance. As a result, HIFs are mainly detected by using the current signals.

The locations of F2 and F5 are considered for the forward and backward faults, respectively. Two HIF scenarios are simulated based on the data given in Table 4. Figs. 6a and 6d illustrate fault current signals considering various parameters of the HIF. As can be seen in Figs. 6b and 6e, in two cases, the MACI signals cross the threshold line in fewer than 5 samples and as a result, the *MACI* identified the fault direction in fewer than 10 samples. Note that the sampling frequency is selected 2 kHz, and so the average required time to detect the direction will be 5 ms.

4.1.6. Performance assessment of the proposed algorithm for different type of DG

Wind energy is one of the main resources to produce electrical energy. Also, owing to the high control capability of DFIGs, they are a very good choice for wind power plants. The fault current of a DFIG can be described as follows [8]:

$$i_R(t) = \frac{\sqrt{2}V_{R(t)}}{(1-s)\sqrt{X(')^2 + R_{cb}{}^2}} e^{\frac{-t}{T_{cb}}} \cos\left((1-s)\omega_s t + \theta_0 - \frac{\pi}{2}\right) - \frac{\sqrt{2}V_{R(t)}}{(1-s)\sqrt{X(')^2 + R_{cb}{}^2}} e^{\frac{-t}{T_a}} cos\left(\theta_0 - \frac{\pi}{2}\right) \quad (16)$$

where V_R shows the pre-fault voltage of phase R, X' is the transient reactance of machine, R_{cb} denotes the crowbar resistance, T_{cb} denotes the transient time constant of the machine, s presents the machine slip, $\omega_s=2\pi f$ shows the angular frequency, f is the nominal frequency of the power system, Ta is stator time constant, and θ_0 is initial phase angle that introduces the instant of fault on the phase R voltage waveform at t = 0. According to (16), the fundamental frequency of stator fault current ($f_{S.F}$) can be presented as follows:

$$f_{S.F} = (1-s)f \quad (17)$$

In a typical DFIG, s may change between -0.2 and +0.3. Thus, considering (17), the fundamental frequency of the stator fault current varies between 35 and 60 Hz for power systems with 50-Hz nominal frequency. Therefore, when a fault occurs, the current injection of DFIG can change the frequency and time characteristics of the grids' current and voltage waveforms. This issue can lead to the malfunction of directional algorithms [8]. Therefore, in this section, the effect of this type of scattered source on the performance of the proposed algorithm is investigated.

It is assumed that a DFIG with a capacity of 1 MW has been replaced with the synchronous generator in the test system of Fig. 3. The details of these distributed generations are presented in [8]. Various scenarios have been simulated in the presence of the DFIG, in which the generator slip, fault resistance, and fault location have been changed. The results are tabulated in Table 5, which confirms the accuracy and speed of the proposed algorithm. The results show that the change in slip and consequently the frequency variation of the DFIG fault current cause no effect on the performance of the proposed algorithm. It should be noted that the nominal frequency deviation from 50 Hz (due to slip changes) reduces the accuracy of the algorithm, but in the worst case, the

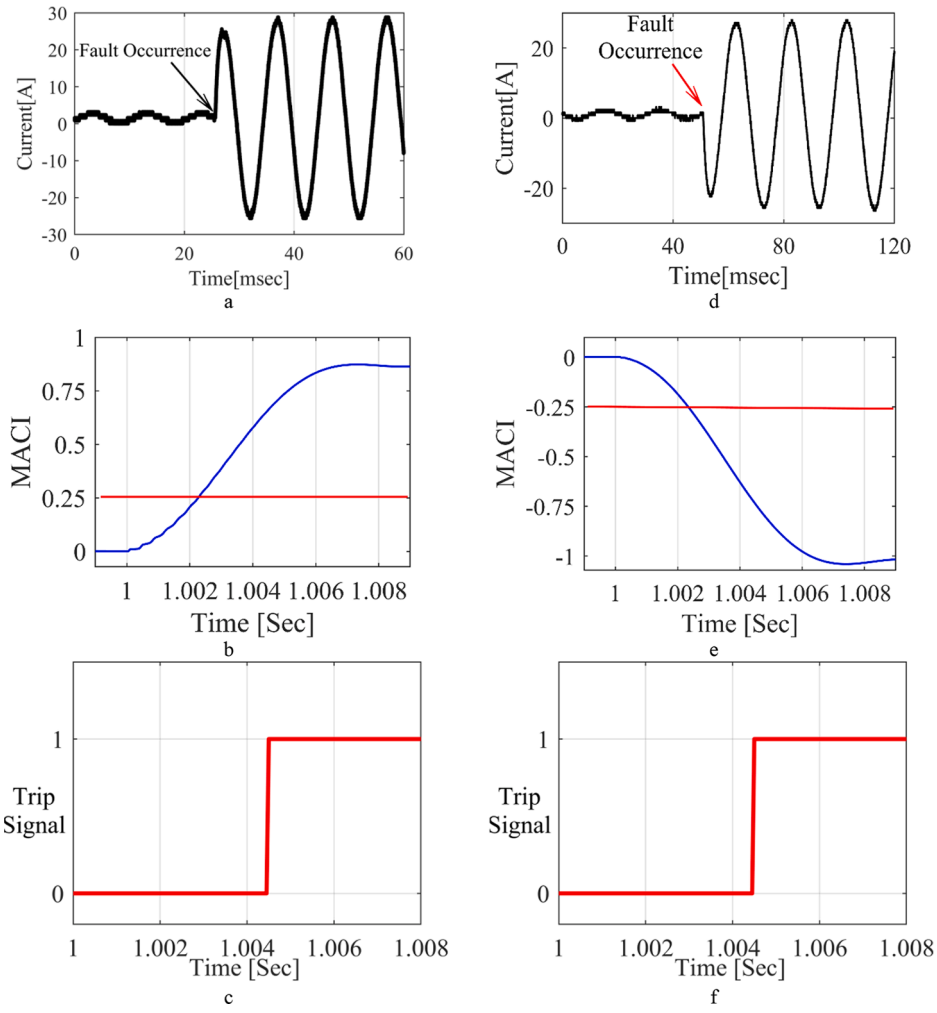

Fig. 17. : Performance evaluation based on experimental recorded fault current signals, (a) forward faults currents, (b) the proposed index for the forward fault currents, (c) detection signal, (d) the backward fault currents, (e) the proposed index for the backward fault currents, (f) detection signal

Table 8
Accuracy of the algorithms

Algorithm	Required Time (ms)		Error (%) Without noise	Error (%) Presence of noise
	Max	Average		
The Algorithm1 [31]	7.2	6.25	1.9	4.6
The Algorithm2 [32]	20	20	1.5	1.8
The Algorithm3 [33]	6.65	5.21	1.8	9.8
Proposed Algorithm	6.7	5.41	1.13	1.23

algorithm has an accuracy greater than 98%.

4.2. Simulation results for 15 buses test system

One of the most important challenges of the protection system in a microgrid is the correct operation of directional relays in the presence of DGs in two modes of grid-connected and islanding of the DGs. For this purpose, in this section, the performance of the proposed algorithm in the 15-bus test system in two modes of grid-connected and islanding of the DGs is investigated.

The single line diagram of the 15-bus test system is shown in Fig. 7. It is connected to the upstream network through bus 8 with a short circuit capacity 200 MVA [27]. The grid has a 5 MW wind turbine and a 20 MW synchronous generator. The details of these distributed generations have been presented in [29]. A directional overcurrent relay is installed at the beginning of the line and between the 14th and 15th buses. In this study, two different locations are considered for fault occurrence; one behind the relay (F2) and one in front of it (F1). In addition to the fault location, the effect of fault resistance, and the slope of DFIG are also assessed. Simulation of each fault location is carried out for three different fault resistances between 0 and 50 Ω. The simulations are performed in two modes of grid-connected and islanding of the DGs. In all cases, the fault is incepted at 1s. In Fig.8, as an example, the simulation results of two forward and two backward faults are provided. Evaluation of Figs. 8c and 8f shows that in both types of faults and in both scenarios (grid--connected and islanding of the DGs), the MACI identifies the fault direction in less than 5 ms.

Also, several numerical results tabulated in Table 6 indicate that the directional algorithm is slower in island mode. The maximum operating time of the algorithm in this mode is 5.70 ms, which is acceptable. Also, slip changes decrease the accuracy of the directional algorithm. But, in this case, the accuracy of the algorithm is always higher than 98%.

4.3. Simulation results for 9 buses IEEE test system

The performance of the proposed fault direction identification index is evaluated for the 9-bus IEEE test system. The test system contains 3 generators, 3 two-winding transformers, 6 lines, and 3 loads. The test

system has voltage levels 13.8 kV, 16.5 kV, 18 kV at the generators' buses, and 230 kV at the other buses. The required data for implementing the test system have been given in [30]. The single-line diagram of this system is shown in Fig. 9. A directional overcurrent relay is installed at the beginning of the line and between buses 8 and 9 at the transmission level. Six fault scenarios according to Table 7, are simulated considering fault resistance variations between 0 and 50 ohms, and two different locations are considered for fault occurrence; one behind the relay and one in front of it.

Figs 10a, 11a and 12 a illustrate forward and backward fault current signals considering various fault resistances. As seen in Figs. 10b, 11b, 12b and 10c, 11c, 12c, in all cases, the MACI signals cross the threshold line in fewer than 6 samples and as a result, the fault direction is identified by the MACI less than 12 samples. Note that the sampling frequency is selected 2 kHz, and so the average required time to detect the direction will be 6 ms. As a result, the proposed method can robustly identify the fault direction in a typical transmission system.

4.4. DSP implementation of the proposed index

This section investigates the performance of the proposed algorithm in digital signal processing (DSP) implementation. To this end, a processor called TMDSCNCD28335 board, which has similar performance compared with the employed processors in protection relays is utilized. Accuracy and speed of the implemented algorithm in practice are the main criteria for judging the performance of the method in practice. A schematic of the employed test bench for evaluation of the method in the real application is shown in Fig. 13. The test bench includes a computer with Ci5-4200U CPU, a TMDSCNCD28335 board, and an oscilloscope to record the toggle signal. The processor has high-performance static CMOS technology – up to 150 MHz (6.67 ns Cycle Time). In addition, it includes 256K $\times$ 16 flash memory and 34K $\times$ 16 SARAM memory on the chip.

During DSP implementation, F1 and F4 faults that are shown in Fig. 3 are considered as forward and backward faults, respectively. The current signals are sent through a serial communication link from PC to DSP with a sampling frequency of 10 kHz. The DSP processes the received data and sends the direction signal to the computer. The toggle signal confirms that the processor can handle the calculations in real-time. Fig. 14 shows the toggle signal steps in each sampling period.

Figs. 15.a and d show the current signals for F1 and F4 faults, respectively. Also, Figs. 15.b and e show the proposed index variations for these two faults. In both cases, the MACI signal crosses the 0.25 and -0.25 threshold lines about 3 ms after the fault occurs for forward and backward fault signals, respectively. Since the MACI remains in the detection areas for a notable time after fault inception, the algorithm correctly identifies the fault direction in both cases provided in Fig. 15. According to the detection signals illustrated Figs. 15.c and e, it can be concluded that the algorithm detects the direction about 6 ms after the fault occurrence.

4.5. Performance evaluation using experimental data

This section provides experimental recorded fault current data for a two sources test system including a three-phase grid supply and asynchronous generator (G1). As shown in Fig. 16, the single line diagram of the experimental setup includes two step-down transformers T1 and T2 to reduce the voltage of the sources. Also, the power grid and the synchronous generator are connected through lines 1 and 2 which are modeled using several resistors and inductors. The fault scenarios are applied at different locations of the lines (F1, F2, and F3) utilizing a two-state switch in series with a high-power resistor. As shown in Fig. 16, the fault current signals are recorded using a data logger at a sampling frequency of 7.812 kHz.

To evaluate the performance of the proposed index, two scenarios are provided in Figs. 17.a and c. As observed in Figs. 17.b and d, the proposed algorithm can identify the fault direction in about 5 ms after fault occurrence in presence of practical noise.

5. Comparison with state-of-the-art

In this section, the performance of the proposed algorithm is compared with three algorithms including the protection algorithm based on auto cosine similarity of feeders current patterns [31], the directional algorithm based on post fault current [32], and amplitude based directional relaying scheme [33]. The comparison is performed from the accuracy, speed, and also robustness in presence of noise aspects. It should be noted that for this comparison the test system given in Fig.3 is used. The simulations performed in this section are performed in two parts. In each part, 100 different case studies have been simulated in which the location, type, and resistance of the fault have been changed. In the first and the second parts, the case studies are simulated with and without the presence of noise, respectively. To investigate the effect of noise, white Gaussian noise with 30 signal-to-noise ratios (SNRs) are added to the simulated current signals. The results of this comparison are summarized in Table 8. The following results can be concluded from this table:

- Algorithm 1: It has acceptable accuracy in the absence of noise, poor performance in the presence of noise. Also, the required average time of this algorithm is about 6 ms, which is slower than the proposed algorithm.
- Algorithm 2: Although the performance of this algorithm in the presence of noise is good, it has a lower speed than the proposed algorithm
- Algorithm 3: The error of the algorithm is higher than 9, which has low inaccuracy comparing with the MACI.

6. Conclusion

Due to the presence of DGs in the distribution network, the protection schemes have been confronted with serious protection challenges. This paper has presented a new directional algorithm based on the rate of change of fault current. The presented algorithm has been designed based on the straightforward formulations that guarantee low response delay, high accuracy, and robustness in presence of noise and the decaying DC component. The proposed algorithm has been evaluated in presence of two types of distributed sources such as synchronous generator and DFIG. Also, the performance of the proposed algorithm under different fault types, fault locations, fault resistances has been evaluated. The performance evaluations under various simulation and experimental scenarios reveal that the proposed algorithm can identify the fault direction in about 5 ms in most cases. Comparing with the previously suggested directional relay algorithms, the proposed method shows higher accuracy, speed, and noise immunity. Furthermore, the proposed method can effectively operate in the transmission system even in the case of high impedance fault resistance. Also, the proposed method can be implemented with low sampling frequency and the mathematics of the proposed algorithm alongside DSP implementation guarantee low computational burden. While the proposed technique works well only for effectively earthed networks, the proposed technique could not handle earth faults in which the fault current is negligible (i.e. unearthed systems). In addition, the proposed technique operates based on the variation of the angles of the fault current before/after fault occurrence. According to the various results, the proposed technique can handle high-impedance fault conditions (low level of fault current). However, in case of earth faults, if the fault current is negligible (i.e. unearthed systems), the proposed technique cannot operate, properly. Overall, the results confirm that the proposed algorithm can be implemented as the fault direction identifier with promising accuracy and speed.

CRediT authorship contribution statement

Mohammad Sadegh Payam: Methodology, Software, Writing – original draft, Writing – review & editing, Visualization, Validation, Formal analysis. **Haidar Samet:** Conceptualization, Methodology, Project administration, Supervision, Writing – review & editing, Data curation. **Teymoor Ghanbari:** Investigation, Project administration, Supervision, Writing – review & editing, Data curation. **Mohsen Tajdinian:** Methodology, Writing – original draft, Writing – review & editing, Validation, Visualization, Formal analysis.

Declaration of competing interest

There is no conflict of interest.

References

[1] F.C.R. Coelho, W. Peres, I.C. Silva Júnior, B.H. Dias, Empirical continuous metaheuristic for multiple distributed generation scheduling considering energy loss minimisation, voltage and unbalance regulatory limits, IET Generat. Trans. Distribut. 14 (16) (2020) 3301–3309.

[2] Q. Cui, X. Bai, W. Dong, Collaborative planning of distributed wind power generation and distribution network with large-scale heat pumps, CSEE J. Power Energy Syst. 5 (3) (2019) 335–347. Sept.

[3] A. Alam, V. Pant, B. Das, Optimal placement of protective devices and switches in a radial distribution system with distributed generation, IET Generat. Trans. Distribut. 14 (21) (2020) 4847–4858.

[4] S. Jamali, H. Borhani-Bahabadi, Recloser time–current–voltage characteristic for fuse saving in distribution networks with DG, IET Generat. Trans. Distribut. 11 (1) (2017) 272–279.

[5] M.E. Hamidi, R.M. Chabanloo, Optimal allocation of distributed generation with optimal sizing of fault current limiter to reduce the impact on distribution networks using NSGA-II, IEEE Syst. J. 13 (2) (2019) 1714–1724. June.

[6] X. Xiao, R. Yang, X. Chen, Z. Zheng, Integrated DFIG protection with a modified SMES-FCL under symmetrical and asymmetrical faults, IEEE Trans. Appl. Supercond. 28 (4) (2018) 1–6. June.

[7] A. Hooshyar, M.A. Azzouz, E.F. El-Saadany, Three-phase fault direction identification for distribution systems with DFIG-based wind DG, IEEE Trans. Sustain. Energy 5 (3) (2014) 747–756. July.

[8] H. Samet, T. Ghanbari, H.J. Ashtiani, M.A. Jarrahi, Evaluation of directional relay algorithms in presence of wind turbines and fault current limiters, Int. Trans. Electric. Energy Syst. (2018) 1–24, https://doi.org/10.1002/etep.2772.

[9] A. Lei, X. Dong, V. Terzija, An Ultra-High-Speed directional relay based on correlation of incremental quantities, IEEE Trans. Power Del. 33 (6) (2018) 2726–2735.

[10] X.Dong Lei, V. Terzija, An Ultra-High-Speed directional relay based on correlation of incremental quantities, IEEE Trans. Power Del. 33 (6) (2018) 2726–2735. Dec.

[11] K.S. Prakash, O.P. Malik, G.S. Hope, Amplitude comparator based algorithm for directional comparison protection of transmission lines, IEEE Trans. Power Deliv. 4 (4) (1989) 2032–2041. Oct.

[12] S.M. Hashemi, M.T. Hagh, H. Seyedi, Transmission-line protection: a directional comparison scheme using the average of superimposed components, IEEE Trans. Power Deliv. 28 (2) (2013) 955–964. April.

[13] D. Prasad, M. Biswal, P.K. Nayak, Swarm assisted positive sequence current component based directional relaying for transmission line protection. 2020 IEEE 9th Power India International Conference (PIICON), SONEPAT, India, 2020, pp. 1–6.

[14] A. Jalilian, M.T. Hagh, S. Hashemi, An innovative directional relaying scheme based on post fault current, IEEE Trans. Power Deliv. 29 (6) (2014) 2640–2647.

[15] P. Valsan, K.S. Swarup, Wavelet transform based digital protection for transmission lines, Int. J. Electr. Power Energy Syst. 31 (7) (2009) 379–388.

[16] Wei Chen, O.P. Malik, Xianggen Yin, Deshu Chen, Zhe Zhang, Study of wavelet-based ultra high speed directional transmission line protection, IEEE Trans. Power Deliv. 18 (4) (2003) 1134–1139. Oct.

[17] U. Lahiri, A.K. Pradhan, S. Mukhopadhyaya, Modular neural network based directional relay for transmission line protection, IEEE Trans. Power Syst. 20 (4) (2005) 2154–2155.

[18] M. Sanaye-Pasand, O.P. Malik, High speed transmission system directional protection using an Elman network, IEEE Trans. Power Deliv. 13 (4) (1993) 1040–1045.

[19] T.S. Sidhu, H. Singh, M.S. Sachdev, An artificial neural network for directional comparison relaying of transmission lines. Sixth Int. Conf. Developments in Power System Protection, Conf. Publ, Nottingham, 1997, pp. 282–285.

[20] T.S. Sidhu, H. Singh, M.S. Sachdev, Design, implementation and testing of an artificial neural network based fault direction discriminator for protecting transmission lines, IEEE Trans. Power Deliv. 10 (2) (1995) 697–706, np.

[21] M. S. Payam, H. Samet and T. Ghanbari, "Instantaneous Frequency-Based Algorithm for Directional Relays," in IEEE Syst. J., doi: 10.1109/JSYST.2020.3029849.

[22] P. Jena, A.K. Pradhan, A Positive-Sequence Directional Relaying Algorithm for Series-Compensated Line, IEEE Trans. Power Deliv. 25 (4) (2010) 2288–2298. Oct.

[23] P.M. Anderson, Power System Protection, IEEE Press, New York, 1999.

[24] P. Jena, A.K. Pradhan, Directional relaying during single-pole tripping using phase change in negative-sequence current, IEEE Trans. Power Deliv. 28 (3) (2013) 1548–1557. July.

[25] H. Samet, T. Ghanbari, M.A. Jarrahi, H.J. Ashtiani, Efficient current-based directional relay algorithm, IEEE Syst. J. 13 (2) (2019) 1262–1272. June.

[26] H. Gao, P.A. Crossley, Design and evaluation of a directional algorithm for transmission-line protection based on positive sequence fault components, IEE Proc.-Gener., Transmiss., Distrib 153 (6) (2006) 711–718.

[27] M E.H. Golshan, S.A. Arefifar, Distributed generation, reactive sources and network-configuration planning for power and energy-loss reduction, IEE Proc. Gener. Trans. Distrib. 153 (2) (2006) 127–136.

[28] M. Wei, W. Liu, F. Shi, H. Zhang, Z. Jin, W. Chen, Distortion-controllable Arc modeling for high impedance Arc fault in the distribution network, IEEE Trans. Power Delivery 36 (1) (2021) 52–63, https://doi.org/10.1109/TPWRD.2020.2981376. Feb.

[29] T. Amraee, Coordination of directional overcurrent relays using seeker algorithm, IEEE Trans. Power Deliv 27 (3) (2012) 1415–1422.

[30] P.M. Anderson, A.A. Fouad, Power System Control and Stability, 2nd ed., IEEE Press, NewYork, 2003.

[31] M.M.A. Mahfouz, A protection scheme for multi-distributed smart microgrid based on autocosine similarity of feeders current patterns, Electric Power Syst. Res. 186 (1) (2020) 1–9.

[32] S.Lotfifard Kiaei, M. Ghanaatian, Current-only directional overcurrent protection using Postfault current. 2019 IEEE Texas Power and Energy Conference (TPEC), College Station, TX, USA, 2019, pp. 1–5.

[33] S. Aktera, S. Biswalb, N.S. Rathore, P. Dasa, A.Y. Abdelazizd, Amplitude based directional relaying scheme for UPFC compensated line during single pole tripping, Electric Power Syst. Res. 184 (2020) 1–14.